SPECIAL PAPER 8

GEOLOGY AND GEOCHEMISTRY OF MT. HOOD VOLCANO

1980

STATE OF OREGON
DEPARTMENT OF GEOLOGY AND MINERAL INDUSTRIES
DONALD A. HULL, STATE GEOLOGIST

STATE OF OREGON
DEPARTMENT OF GEOLOGY AND MINERAL INDUSTRIES
1069 State Office Building, Portland, Oregon 97201

Special Paper 8

GEOLOGY AND GEOCHEMISTRY OF MT. HOOD VOLCANO

CRAIG WHITE
Department of Geology, University of Oregon

1980

Conducted in conformance with ORS 516.030
Funded in part under U. S. Department
of Energy Contract EG-77-C-06-1040

C O N T E N T S

I L L U S T R A T I O N S

Figures:

Tables:

Cover:

Main Stage lava flows mantled by glacial till on the eastern side of Mt. Hood.

ABSTRACT

The lavas that comprise Mt. Hood volcano can be divided on the basis of their age and modal composition into three suites. These are: (1) the sequence of pyroxene and hornblende andesites that was erupted prior to the last glaciation and which makes up about 90 percent of the volcano; (2) the post-glacial hornblende dacites that were erupted primarily as hot avalanche flows from domes near the summit; and (3) the flows of olivine andesite that were erupted from several satellite vents on the flanks of Mt. Hood. This paper presents new compositional data for the Main Stage lavas and the post-glacial dacites.

Eruption of the post-glacial dacites took place during three episodes at approximately 10,000 yrs., 2,000 yrs., and 200 yrs. b. p. Each eruptive episode produced a geochemically distinct series of lavas. Within each age group, sequentially erupted lavas appear to be related by small degrees of fractionation of the observed phenocryst phases. Estimates of the conditions of equilibration of the post-glacial dacites were made by comparing the phenocryst compositions in a dacite sample with experimental equilibria data. The calculations yielded the following results: temperature = 935° C $\pm$ 35°; logarithm of oxygen fugacity = -10.2 to -9.6; minimum load pressure = 2.5 to 3.5 kb (approximately equal to 7 to 10 kilometers depth).

Samples of Main Stage lavas were taken from five sub-aerial flow sequences and the Timberline drill hole. Major and trace element analyses indicate that the sequentially erupted lavas in any one section are not related as members of a simple fractional crystallization series. The occurrence of siliceous lavas near the base of some sections indicates that Main Stage magma reservoirs may have been compositionally zoned. It is suggested that the contrasting processes of differentiation indicated for the post-glacial versus the Main Stage magmas (fractional crystallization vs. magma zonation) may be related to the considerable differences in volumes and cooling rates inferred for their respective reservoirs. When the trace element abundances in all Main Stage lavas are compared, at least two discrete magma batches can be identified.

Because of the inferred small volumes and deep residence levels of the post-glacial magma reservoirs, it is unlikely that they would generate a significant geothermal anomaly within or immediately beneath Mt. Hood. Nonetheless, because of the very young age of the most recent eruptions (100 to 200 yrs. b. p.), a local heat source could be provided by magma that is still residing at shallow depths within the volcanic conduit. In addition, deep-seated magma chambers associated with either post-glacial or Main Stage volcanism could continue to affect the regional geothermal gradient in the vicinity of Mt. Hood.

GEOLOGY AND GEOCHEMISTRY OF MT. HOOD VOLCANO

INTRODUCTION

Mt. Hood is the northernmost of the large composite volcanoes that form the crest of the Cascade Range in Oregon. The volcano is predominantly andesitic in composition and consists of about 180 cubic kilometers of flows and pyroclastic debris. The last major eruption at Mt. Hood took place about 200 years ago; however, minor activity was reported as recently as 1865. The continued presence of fumeroles near the summit of Mt. Hood indicates that the volcano is still active.

In his major study of the Mt. Hood area, Wise (1969) divided the volcano into three lava groups; a voluminous series of andesitic lavas that was erupted prior to the last glaciation, a post-glacial group of dacitic plug domes and pyroclastic flows, and several post-glacial satellite cones of olivine andesite. Crandall and Rubin (1977) subdivided the dacitic rocks by delineating three age units within the pyroclastic facies. The lowermost block and ash flows are interbedded with glacial till and outwash, and on this basis, their age is estimated to be about 10,000 to 12,000 years BP. These flows are overlain by two younger pyroclastic sequences that contain charcoal which have yielded radiocarbon dates of 1,700 years and 200 years BP.

For this report, the pre-glacial Mt. Hood sequence will be called the Main Stage lavas and the post-glacial silicic rocks will generally be referred to as dacites, although some andesitic rocks do occur in the sequence. The names, Polallie, Timberline, and Old Maid Flat have been applied by Crandall (pers. comm.) to the 10,000-12,000 yr, 1,700 yr, and 200 yr-old block and ash flows, respectively, and these names will be used in place of the absolute age designations.

Scope

The present study was initiated in order to apply recently developed techniques in petrology and geochemistry to the problem of the late-stage magmatic evolution of the Mt. Hood lavas. Because knowledge of the order of eruption of lavas is critical in evaluating competing petrological models, new analyses of rock samples have been made only where the relative ages of flows in a section have been determined by the field observation, drilling, or radiometric dating. The goal of the study is to aid in the assessment of Mt. Hood as a potential geothermal resource area and, for this reason, emphasis has been placed on the evolution of the young, silicic rocks, even though they are volumetrically less important than the Main Stage lavas.

Analytical Procedures

Concentrations of eight major elements in all the Mt. Hood samples were determined by X-ray fluorescence spectrometry of fused glass discs. Sample splits were analyzed for Na and Mg by use of a Varian model 175 atomic absorption unit. Zr, Sr, Rb, and Ni concentrations were determined by X-ray fluorescence analysis of pressed powders; all other trace element analyses were made by use of instrumental neutron activation. Complete trace element analyses were made by counting irradiated samples for two and six hours on a 4096 channel germanium crystal detector. Less precise analyses were obtained for most of the dacitic rocks by counting samples for two hours on a 2048 channel detector; a procedure that is more rapid and less costly than that used for the complete analyses but which yielded reliable values for Th and La. Mineral analyses were made with an electron microprobe.

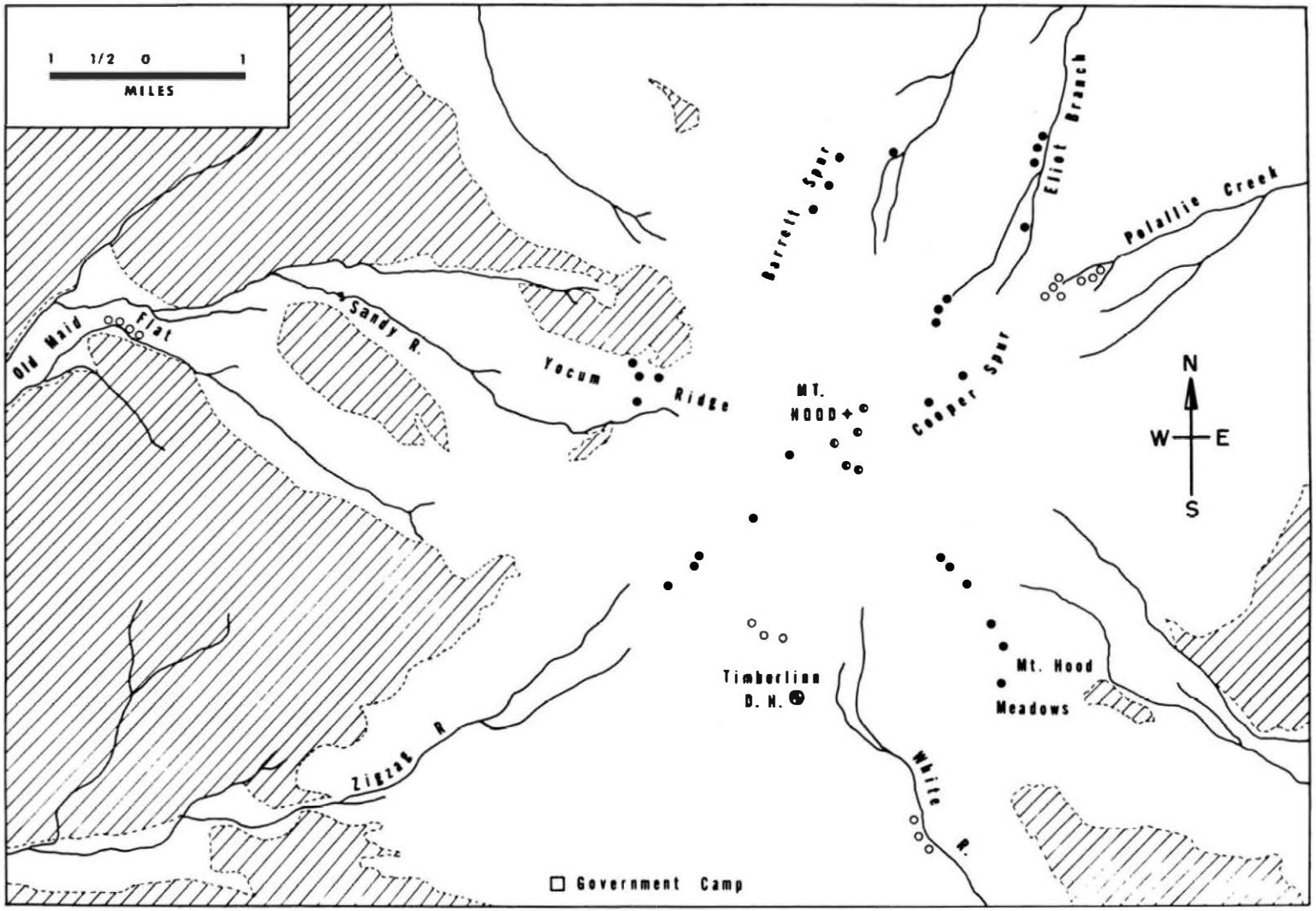

Figure 1: Index map of the Mt. Hood area. The distribution of pre-Mt. Hood rocks is indicated by the diagonal ruling. The locations of chemically analyzed specimens are shown by the circular symbols; filled circles for Main Stage lavas, half-filled circles for near-summit dacitic flows and plugs, and open circles for blocks in dacitic block and ash flows.

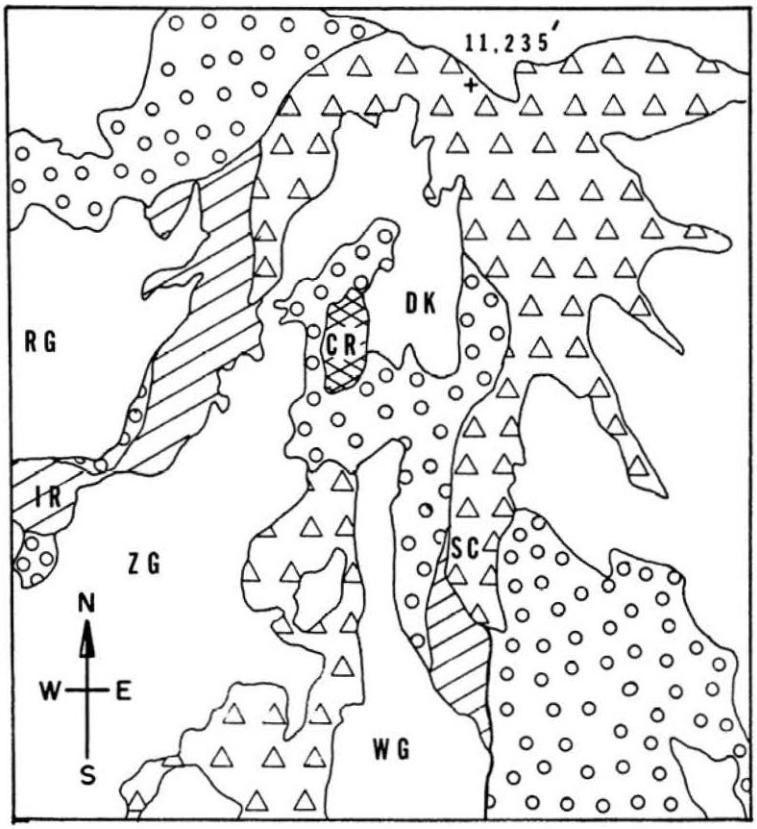

Snow and ice

Moraine

Plug dome;
hornblende dacite

Flows or crumble breccia;
hornblende dacite

Main Stage lava flows;
hornblende or pyroxene andesite

CR Crater Rock
DK Devils Kitchen
IR Illumination Rock
SC Steel Cliff
WG White River Glacier
ZG Zigzag Glacier
RG Reid Glacier

scale:

2,000 ft.

Figure 2: Geological sketch map of the summit area of Mt. Hood.

POST-GLACIAL DACITES

Post-glacial dacitic lavas at Mt. Hood occur primarily as voluminous pyroclastic debris flows which fill radial drainages and mantle the lower slopes of the volcano. The abundance of prismatically jointed blocks throughout the pyroclastic section and the uniform magnetic orientation of blocks in some flows indicate that most of the debris was deposited at elevated temperature; in some cases at temperatures above the Curie point. The flows probably originated from explosive eruptions at the sides or base of an episodically active dome, the remnants of which cap most of the near-summit ridges.

The Polallie block and ash flows are the oldest and most voluminous of the post-glacial pyroclastic deposits. They occur primarily on the east and northeast sides of the volcano where they are well exposed in sections up to 150 meters thick in the canyons of Polallie and Cold Spring Creeks (Figure 1). Flows of Polallie age have not been identified on the south, west, or northwest slopes of Mt. Hood. A crumble-breccia that occurs at the 9500-foot level on Cooper Spur may represent part of the Polallie dome that was undermined by the repeated block and ash eruptions.

In contrast to the Polallie eruptions, the explosive activity that produced the Timberline and Old Maid Flat flows was strongly directed to the south and west. The 1,700-year-old Timberline pyroclastic flows mantle the south slope of Mt. Hood in the vicinity of Timberline Lodge and form thick sections in the upper reaches of the Zigzag and Sandy Rivers. The 200-year-old flows of the Old Maid Flat group overlie flows of Timberline age in exposures along the Sandy River where a twenty-centimeter-thick ash layer marks the contact. It is likely that rocks of Old Maid Flat age also form the noticeably steeper portion of the south slope between the 8000-foot level and the base of Crater Rock. The large blocks in this area are similar in their mineralogical and chemical composition to blocks from other Old Maid Flat sections and they probably were formed by the collapse of a young dome that occupied the Devils Kitchen amphitheater, just south of the present summit (Figure 2).

The hornblende dacite plug dome that forms Crater Rock is the site of the most intense fumarolic activity in the summit region. Its extrusion probably followed the explosive activity that produced the Old Maid Flat flows and caused the collapse of the Devils Kitchen dome. Additional evidence of very young activity was found by Crandall (pers. comm., 1979), who recognized small pumice fragments on the surface of the Old Maid Flat flows in the upper portions of the White River valley. The pumice is unlike that erupted from neighboring volcanoes and was almost certainly produced by a minor eruption of Mt. Hood, possibly during the reported activity in the middle 1800s.

Petrography

All of the post-glacial dacitic rocks at Mt. Hood contain abundant phenocrysts of plagioclase and ferromagnesian minerals in a groundmass of fine-grained crystals, crypto-crystalline material and, rarely, light brown glass. Phenocrysts and microphenocrysts of plagioclase and orthopyroxene $\pm$ amphibole $\pm$ clinopyroxene form between 30 and 35 percent of the mode in nearly all observed samples.

Although most phenocryst grains are optically zoned, the range of mineral compositions as revealed by the electron microprobe is relatively narrow. Most phenocrysts are fresh and display subhedral or euhedral crystal outlines; however, amphibole grains are commonly rimmed by fine-grained aggregates of opaque minerals and, in some rocks, may be totally replaced by this material. Clinopyroxene is generally the smallest and least abundant of the phenocryst minerals and its occurrence in a given specimen appears to be inversely related to the abundance of hornblende.

It would be impossible to assign a specimen to one of the three age groups on the basis of petrography alone; nonetheless, general petrographic characteristics can be recognized in each of the pyroclastic units. Blocks from the Polallie flows commonly contain much less modal amphibole and greater amounts of modal clinopyroxene than blocks

from the two younger units. In addition, amphibole phenocrysts are generally quite fresh in the Old Maid Flat blocks but appear to be progressively more resorbed in the older units. These characteristics may reflect the small but progressive increase in the silica contents of the post-glacial dacitic rocks with time.

Geochemistry

The major and trace element compositions of 27 post-glacial silicic lavas from Mt. Hood are given in Table 1. Although some overlap in major elements does occur among the three age groups, a general trend can be seen in which rocks from the younger units are slightly richer in SiO_2 and poorer in MgO, CaO, and Fe_2O_3.

In contrast to the major elements, the concentrations of K_2O, Zr, Th, and La bear a more complex relationship to the age of the sampled unit. This behavior is illustrated in Figure 3, in which the abundances of the four excluded elements are plotted versus a schematic scale of decreasing age. Because the Polallie canyon exposure offered the opportunity to sample a thick continuous section, the samples of Polallie age have been plotted in five positions, according to their stratigraphic height. In contrast, the stratigraphic position of the Timberline and Old Maid Flat samples within their respective units cannot be determined in the field, and for this reason, analyses of these rocks are plotted as if they were exactly time-equivalent. Analyses of the Crater Rock plug dome and the post-Old Maid Flat-age pumice are plotted as the youngest samples.

Examination of the lower portion of Figure 3 reveals a general trend of increasing K_2O, Zr, Th and La upward through the Polallie Canyon section. In a similar way, the Old Maid Flat--Crater Rock--pumice samples show an increase in excluded element concentrations with time. This trend is reversed at the major time breaks where the initial products of each eruptive episode are depleted in these elements relative to the last-erupted lavas of the preceding episode.

The trends within the Polallie section and the Old Maid Flat-Crater Rock-Pumice lava group are consistent with small degrees of fractional crystallization; however, the occurrence of a geochemical reversal at each of the major time breaks indicates that the Polallie, Timberline and Old Maid Flat lavas are probably not related to one another through a simple Bowen-type fractionation process. Because the younger rocks are neither less siliceous nor more phenocryst rich than the older ones, it is also unlikely that the three eruptive groups are related through progressively deeper tapping of a simply zoned magma chamber. Although a single, complexly zoned magma chamber cannot be ruled out as a source of all of the post-glacial dacitic lavas, it is more likely that each of the three major eruptive episodes tapped discrete magma batches. The distinct geochemical character of the lavas of each eruptive episode is emphasized by plotting the excluded elements versus silica. Plots of potash and thorium values are shown in Figure 4.

In summary, the geochemical data from the post-glacial silicic lavas indicate that eruptions of discrete magma batches took place at 12,000-10,000 yrs, 1,700 yrs, and 200 yrs BP. Because the lavas are very similar in mineralogical and major-element chemical composition, it is likely that successive magma batches equilibrated under similar conditions. During each eruptive episode the magmas were differentiated to a small degree by the removal of phenocryst minerals from the melt.

Conditions of equilibration

The temperature, pressure, water content, and oxygen fugacity of the dacitic magmas can be estimated by comparing the mineral compositions of the natural rocks with experimental data on crystal-crystal and crystal-liquid equilibria. A sample (CR-55A) from a prismatically jointed block near the middle of the Polallie Canyon section was selected for these calculations and an extensive analysis was made of its phenocryst and groundmass phases (Table 2).

Table 1. Major and trace element analyses of post-glacial dacites

	Blocks in Polallie Pyroclastic Flows							Blocks in Timberline Pyroclastic Flows				
	HD-83	HD-84	CR-55A	HD-85	HD-4	HD-5	HD-6	HD-17	HD-18	HD-19	HD-26	HD-27
SiO_2	61.99	61.93	61.26	62.73	62.56	62.82	62.90	63.19	63.26	62.91	63.58	63.56
TiO_2	.74	.78	.74	.77	.75	.76	.76	.71	.72	.71	.70	.70
Al_2O_3	17.52	17.65	19.17	17.42	17.05	17.13	17.04	17.00	16.99	17.06	16.92	16.89
MgO	2.71	2.41	2.28	1.68	2.41	2.30	2.26	2.40	2.34	2.43	2.29	2.35
Fe_2O_3	5.90	5.68	5.42	5.74	5.50	5.82	5.44	5.36	5.34	5.38	5.16	5.13
MnO	.09	.09	.07	.09	.07	.07	.07	.07	.08	.07	.07	.07
CaO	5.53	5.67	5.36	5.60	5.46	5.42	5.40	5.45	5.36	5.36	5.22	5.25
Na_2O	3.97	4.26	3.86	4.21	4.41	4.17	4.36	4.17	4.24	4.44	4.39	4.42
K_2O	1.39	1.39	1.65	1.55	1.59	1.63	1.59	1.49	1.52	1.50	1.53	1.49
P_2O_5	.17	.16	.18	.20	.19	.19	.18	.15	.15	.14	.13	.15
Rb	22	21	26	26	27	25	27	20	21	21	22	23
Sr	672	626	609	621	600	596	598	572	579	562	537	557
Zr	143	144	169	156	179	176	175	146	159	152	152	154
Th	3.5	3.3	4.1	4.5	4.3	5.3	n.d.	2.9	n.d.	n.d.	3.0	3.5
La	18.3	18.3	20.2	22.2	22.2	22.2	n.d.	16.8	n.d.	n.d.	15.6	18.2

Note: All major element analyses have been recalculated to 100 percent, water free. Polallie-age blocks were collected in the Polallie Creek area; Timberline-age blocks were collected on the south slope near Timberline Lodge (HD-17,18,19) and along the Sandy River at Old Maid Flat (HD-26,27).

Table 1--Continued

	Basal Old Maid Flat Ash	Blocks in Old Maid Flat Pyroclastic Flows					Near-Summit Dacite Flows				Crater Rock	Pumice
	HD-48	HD-2	HD-28	HD-29	HD-30	HD-31	HD-23	HD-25	HD-8	HD-60	HD-9	HD-10
SiO_2	60.70	63.77	63.26	63.34	63.22	63.49	62.40	62.26	62.76	62.93	64.11	62.88
TiO_2	.86	.72	.71	.72	.72	.71	.77	.78	.77	.80	.69	.73
Al_2O_3	17.35	16.84	17.27	17.11	17.06	16.95	17.25	17.16	17.11	17.67	16.94	17.71
M_9O	3.01	2.24	2.21	2.26	2.36	2.28	2.40	2.45	2.42	2.24	2.11	2.18
Fe_2O_3	6.28	5.26	5.17	5.29	5.26	5.18	5.72	5.68	5.59	5.44	5.12	5.36
MnO	.09	.07	.07	.07	.08	.07	.08	.08	.08	.08	.08	.08
CaO	5.98	5.16	5.30	5.29	5.25	5.18	5.44	5.41	5.46	5.59	5.10	5.30
Na_2O	4.21	4.37	4.48	4.35	4.48	4.56	4.40	4.68	4.19	3.53	4.21	4.08
K_2O	1.34	1.43	1.39	1.42	1.41	1.44	1.38	1.32	1.43	1.54	1.49	1.50
P_2O_5	.18	.15	.14	.15	.15	.14	.17	.18	.17	.18	.15	.19
Rb	19	22	17	20	20	20	18	18	21	24	23	21
Sr	633	552	558	551	555	546	550	545	555	561	534	545
Zr	155	137	140	146	145	145	163	151	160	149	148	174
Th	n.d.	2.9	2.6	n.d.	2.7	n.d.	2.9	n.d.	n.d.	n.d.	3.3	3.8
La	n.d.	15.9	15.6	n.d.	14.0	n.d.	16.7	n.d.	n.d.	n.d.	15.8	17.7

Note: All major element analyses have been recalculated to 100 percent, water free. Old Maid Flat-Age blocks were collected along the Sandy River at Old Maid Flat (HD-28,29) and along the White River (HD-2,30,31).

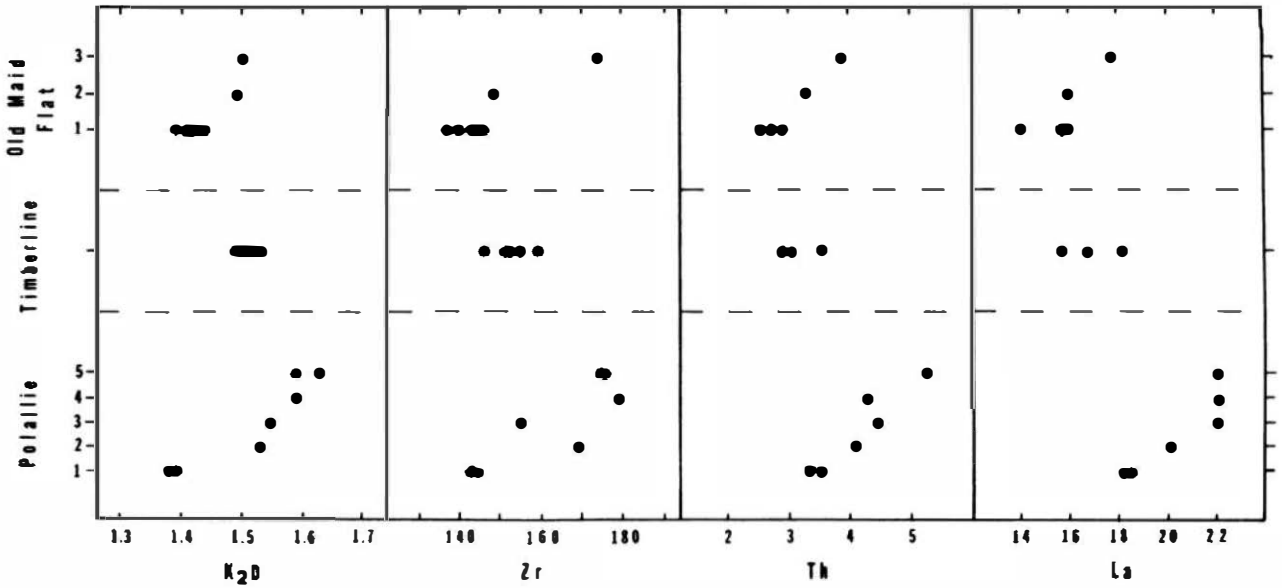

Figure 3: A plot of the concentrations of K_2O (wt %), zirconium (ppm), thorium (ppm), and lanthanum (ppm) in post-glacial dacites versus a schematic scale of stratigraphic height.

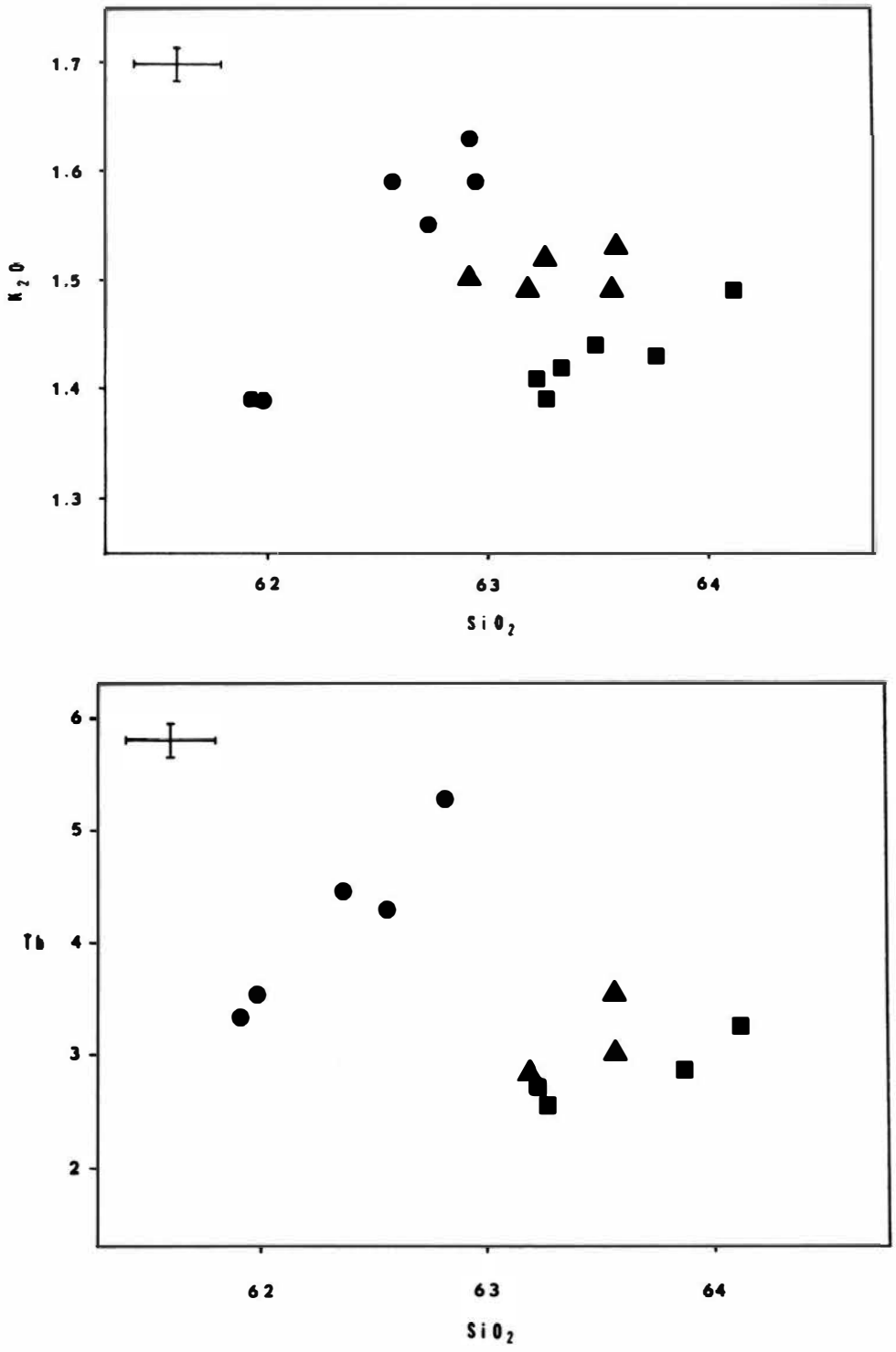

Figure 4: A plot of the concentrations of K_2O (wt %) and thorium (ppm) in post-glacial dacites versus weight percent silica. Circular symbols are used for analyses of Polallie-age blocks, triangles for Timberline-age blocks, and squares for Old Maid Flat-age blocks. 1 sigma error bars are given.

Table 2. Mineral compositions used in equilibria calculations

Pyroxenes	core opx A	core cpx A	rim opx A	rim cpx A	gr mass opx B	gr mass cpx B
SiO_2	52.62	52.10	52.54	52.45	52.82	51.83
TiO_2	.05	.34	.05	.39	.17	.51
Al_2O_3	.67	1.73	.84	1.45	.96	2.04
FeO	22.66	9.12	21.25	9.15	22.63	8.91
MgO	22.90	14.57	22.64	14.77	22.30	14.33
MnO	.69	.28	.68	.28	.65	.25
CaO	1.11	21.70	1.25	21.70	1.19	21.39
Total	100.70	99.85	99.25	100.18	100.71	99.26
EN	65	14	67	14	65	14
FS	35	42	33	42	35	42
WO	--	44	--	44	--	44

Plagioclases	core plag A	rim plag A	core plag B	rim plag B	gr mass plag C	gr mass plag D
SiO_2	56.45	54.53	56.39	54.45	54.19	54.34
Al_2O_3	27.07	28.14	26.96	28.13	28.54	28.13
FeO	.32	.41	.26	.45	.38	.53
MgO	.10	.11	.08	.12	.11	.09
CaO	9.52	10.55	9.55	10.67	11.16	10.89
Na_2O	5.79	5.31	5.92	5.22	5.18	5.20
K_2O	.19	.18	.23	.20	.16	.20
total	99.44	99.23	99.41	99.29	99.75	99.35
AN	48	52	47	53	54	54

Oxides	ilm A	ilm B	ilm C	mt A	mt B
SiO_2	.02	.31	.31	.80	.69
TiO_2	39.90	35.95	39.04	4.54	8.21
Al_2O_3	.29	.50	.45	2.78	2.22
FeO	56.50	60.06	56.04	84.44	82.13
MgO	2.80	2.32	2.88	1.88	2.06
MnO	.10	.06	.08	.14	.14
Cr_2O_3	.06	.08	.07	.26	.26
V_2O_3	.71	.87	.68	.39	.39
total	100.39	100.19	99.55	95.30	96.17
Hematite	27	34	28	--	--
Ilmenite	73	66	72	--	--
Magnetite	--	--	--	85	75
Ulvospinel	--	--	--	15	25

Note: All analyses were made with an electron microprobe using a 3 micron beam width. All phases are from sample CR-55A; a prismatically jointed block from near the middle of the Polallie Canyon section.

Iron-titanium oxide geothermometer: The iron-titanium oxide geothermometer utilizes the co-existing solid-solution phases ulvospinel-magnetite and ilmenite-hematite. When these minerals crystallize under equilibrium conditions, their compositions are uniquely determined by both temperature and the fugacity of oxygen (fO_2). Buddington and Lindsley (1964) published a series of calibration curves from which the temperature and the logarithm of fO_2 of a system can be estimated from the mole fraction of hematite and ulvospinel in the co-existing oxide phases.

When the compositions of these minerals in sample CR-55A are compared with the curves in Figure 5, it can be seen that the ilmenite solid-solution ratio falls outside the range calibrated by Buddington and Lindsley. Nonetheless, the temperature and logarithm of fO_2 of the Polallie magma can be estimated by making a judicious interpolation of the curves. The values obtained from these data are:

$$\text{Temperature} = 935^\circ \pm 35^\circ$$

$$-\log fO_2 = 10.2 - 9.6$$

Pyroxene geothermometer: Distribution of the component $Mg_2Si_2O_6$ between calcium-rich pyroxene and magnesian orthopyroxene has been shown to be temperature dependent. Because they are relatively unaffected by pressure, the compositions of co-existing pyroxenes in the igneous rocks can be used as a geothermometer. From experimental equilibria studies, Wood and Banno (1973) showed that temperature is related to simple pyroxene compositions by

$$T(^\circ K) = \frac{-10202}{\ln(X^{cpx}_{Mg_2Si_2O_6}/X^{opx}_{Mg_2Si_2O_6}) - 7.65\,X^{opx}_{Fe} + 3.88(X^{opx}_{Fe})^2 - 4.6}$$

When the compositions of three pyroxene pairs from sample CR-55A (Table 2) are substituted in the above equation, the calculated temperatures are:

Pyroxene cores	910° C
Pyroxene rims	920° C
Groundmass pyroxenes	918° C

The temperatures fall within a remarkably narrow range and, although they may be somewhat low for low-silica dacites, they are in general agreement with those obtained from the iron-titanium oxides.

Plagioclase geothermometer: The compositional dependence of plagioclase on both temperature and water pressure has long been established by petrologists. Kudo and Weill (1970) successfully formulated an expression by which this relationship could be used to determine the equilibration temperature of plagioclase-liquid pairs at several different water pressures. If temperature can be estimated by an independent method, then the Kudo-Weill equations can be used to estimate the partial pressure of water in a magma at the time of plagioclase crystallization.

The temperatures obtained by the Kudo-Weill method for sample CR-55A, listed as a function of water pressure, are:

P_{H_2O}	Dry	0.5 kb	1.0 kb	5.0 kb
$T^\circ C$ (rim)	1148	1095	1057	765
$T^\circ C$ (core)	1178	1129	1091	803

An estimate of P_{H_2O} can be made from these data by interpolating the values in the temperature range of 900° to 970° C (Figure 6). This procedure yields P_{H_2O} values of approximately 2.5 to 3.5 kb.

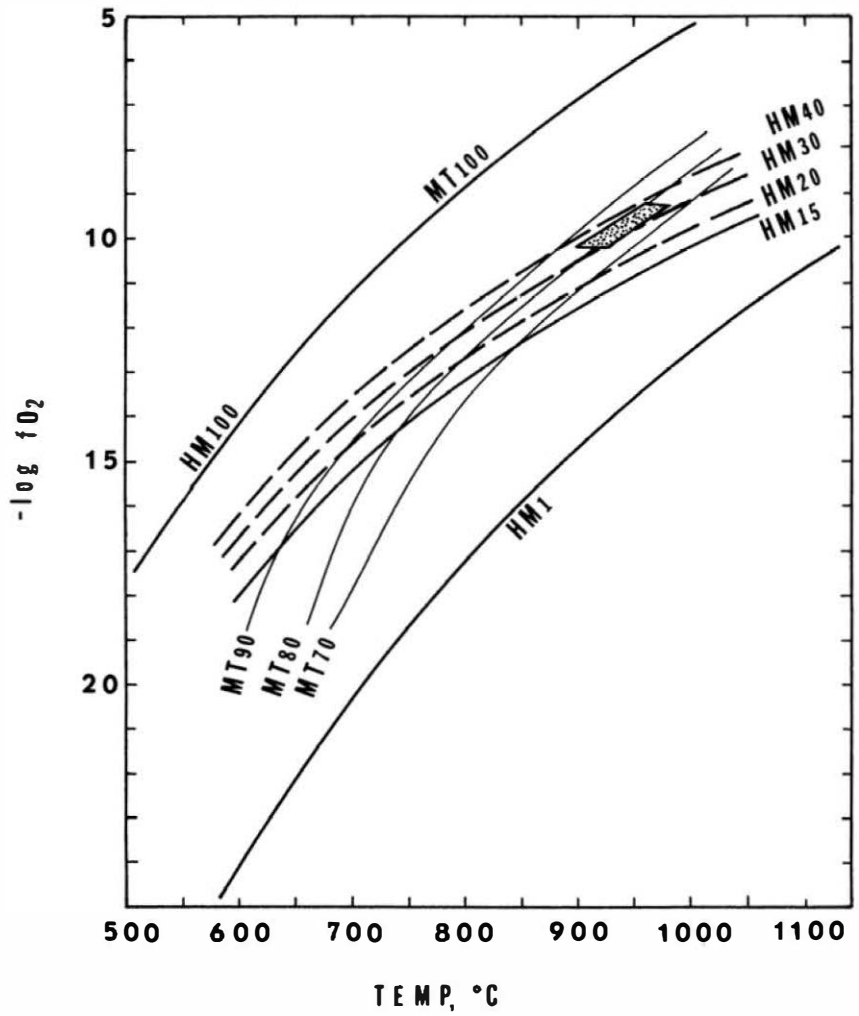

Figure 5: Compositions, in mole percent, of coexisting ilmenite-hematite and magnetite-ulvospinel solid solutions as a function of temperature and oxygen fugacity (after Buddington and Lindsley, 1964). The stippled area shows the compositional range of the oxide phases in sample CR-55A.

Because the partial pressure of water in a magma cannot normally be greater than the total load pressure, the P_{H_2O} estimates represent the lowest pressures at which the Polallie magma could have equilibrated with plagioclase. If the magma was not water saturated, then P_{total} would, of course, have to be greater than 2.5-3.5 kb, and the depth of the magma chamber would exceed 8 to 10 kilometers.

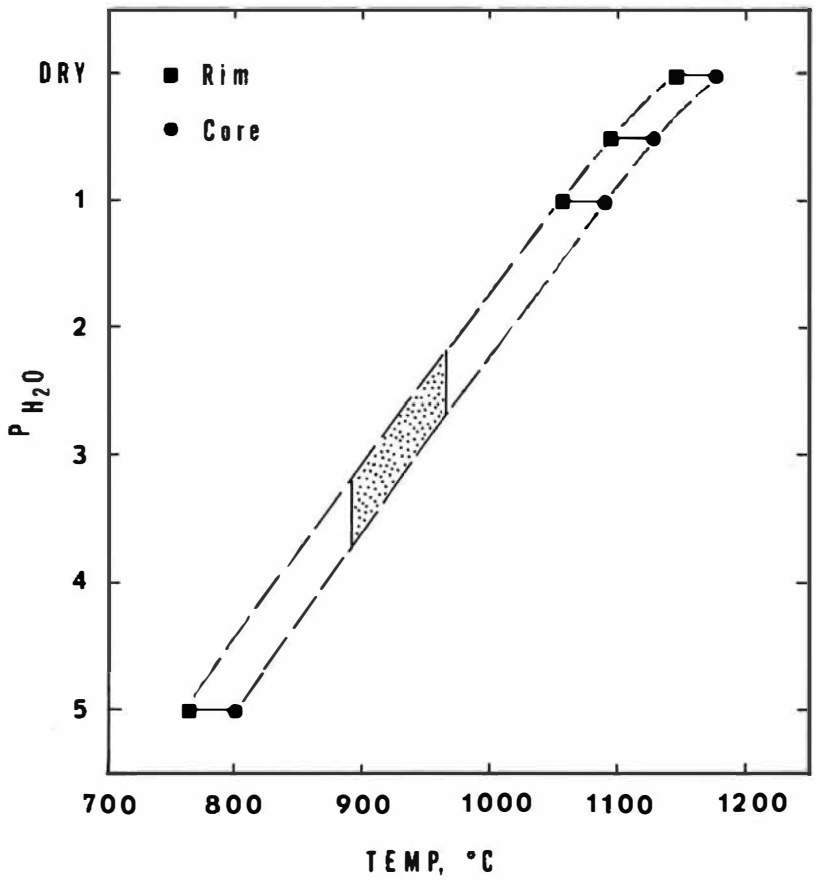

Figure 6: The temperature of equilibration of plagioclase phenocrysts in sample CR-55A shown as a function of water pressure (after Kudo and Weill, 1970). The stippled area shows the temperature range indicated by the two-oxide geothermometer.

MAIN STAGE LAVAS

More than 90 percent of the volume of Mt. Hood volcano is composed of a preglacial series of flows, breccias, and pyroclastic rocks; the great majority of which are andesitic in composition. Unlike the composite cones of the central Oregon Cascade Range, Mt. Hood is not built on an extensive platform of Pleistocene basaltic flows, but rather rests directly on volcanic rocks of Pliocene and Miocene age. The age of Mt. Hood volcano is not known; however, because lavas having reversed remanent magnetism have not yet been found, an age of 660,000 yrs should be considered as a maximum date for the onset of eruption.

In order to understand the magmatic evolution of the Main Stage lavas, surface samples were taken for analysis only where four or more flows could be sampled in unambiguous stratigraphic order. In addition, the Timberline drill hole (3S/9E-7aac) offered a unique opportunity to sample eleven flows through a vertical section of about 1,400 feet.

Petrography

All of the observed Main Stage lavas contain phenocrysts of plagioclase, orthopyroxene and, in lesser abundance, clinopyroxene. Amphibole occurs in about 66 percent of the samples and is generally partially or completely replaced by pseudomorphic mats of fine-grained opaque minerals. In contrast to the observation by Wise (1969) that amphibole-bearing andesite flows occur only in the upper portion of the volcano, the present study indicates that there is no relationship between the stratigraphic height of a flow and its amphibole content. Microprobe analyses were not made of phenocryst phases in the Main Stage lavas; however, mineral analyses and petrographic descriptions are presented by Wise (1969) and a flow-by-flow description of the cuttings from the Timberline drill hole is given in Figure 7.

Geochemistry

The major and trace element composition of samples from six sections and the Timberline drill hole are given in Table 3. The analyses in each set are presented in order of increasing stratigraphic height. The drill hole samples probably represent a complete flow sequence; however, because of lack of continuous exposure, it is unlikely that all flows in the subaerial sections have been sampled.

Major elements: In contrast to the post-glacial silicic lavas, the Main Stage flows show little systematic chemical variation through individual measured sections. The behavior of silica in six sections is given as an example in Figure 8. Although it is clear from this figure that there is no serial variation of SiO_2 concentrations upward through the sections, there is a general tendency for the flows at the lowest projected stratigraphic elevations (< 4900 ft) to be relatively enriched in silica (>62% SiO_2).

The occurrence of siliceous rocks near the base of the Mt. Hood section is inconsistent with a Bowen-type model of fractional crystallization; however, numerous other examples exist of volcanoes in which the initial eruptions produced the most siliceous lavas in a sequence. At Hekla volcano in Iceland, this cycle has been repeated many times and the silica content of the initial products of each eruptive episode has been shown to be proportional to the length of the quiescent period between eruptions (Thorarinsson, 1954). An analysis of this kind cannot be made for the Main Stage Mt. Hood lavas because the absolute time intervals between eruptions are not known. Nonetheless, the eruption of siliceous lavas during the earliest stages of volcanism indicates that at least the initial magma chamber beneath Mt. Hood was compositionally zoned. The recurrence of rocks of dacitic composition at higher intervals in the Main Stage sequence may mark the initiation of later eruptive episodes.

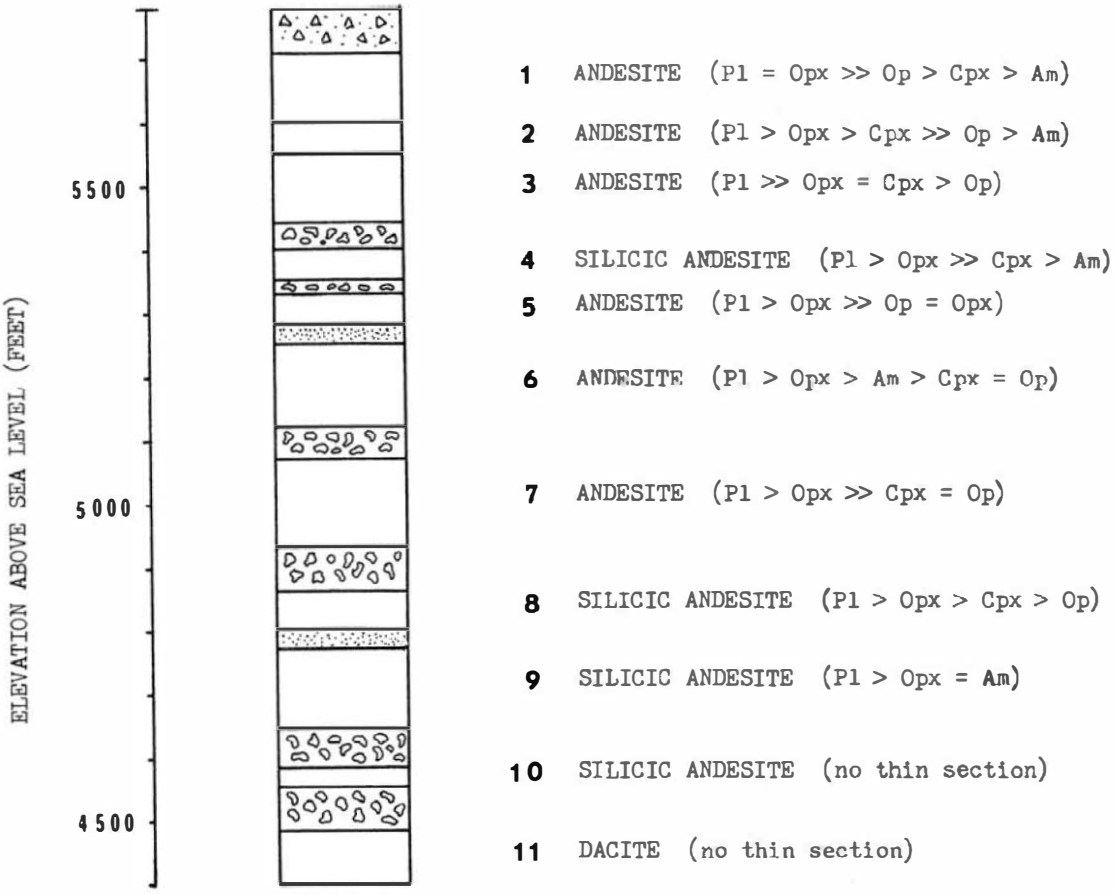

Figure 7: Columnar section in the Timberline Lodge area as indicated by drill hole cuttings. Lava flows are identified by sample number and the relative modal phenocryst abundances are given.

Trace elements: In general, the trace element compositions of the Main Stage lavas tend to reflect the major element contents in any one section of the flows. This tendency can be seen by comparing the major element trends in Figure 9 with the trends for selected trace elements given in Figure 10. As might be expected, the excluded trace elements mimic the silica trend whereas the trends of Ni, Co, and Sc are similar to that of magnesia. The relatively consistent covariation of the major and trace elements in the drill hole section indicates that these flows may be genetically related, perhaps as differentiates of a common parental melt.

When the trace element compositions of flows from different sections are compared, chemical differences appear that cannot be readily explained by late stage differentiation processes. As shown by Figure 11, some flows are noticeably enriched in K_2O and the excluded trace elements compared to other Main Stage lavas with similar major element compositions. With the exception of the basal flow (HD-66), the lavas in the Eliot Branch-Cooper Spur section have the highest excluded element contents whereas the Timberline drill hole samples contain the lowest concentrations of these elements. Flows from other sections fall within one or the other of these trends or occupy intermediate positions.

The existence of geochemically distinct lava suites in asymmetrical distribution around the volcano indicates that Mt. Hood was probably built by periodic eruptions of

Table 3. Major and trace element analyses of Main Stage lavas

	Timberline Drill Hole										
	TDH-11	TDH-10	TDH-9	TDH-8	TDH-7	TDH-6	TDH-5	TDH-4	TDH-3	TDH-2	TDH-1
SiO_2	64.79	62.03	63.71	62.30	60.73	61.90	61.11	62.33	60.77	59.89	59.73
TiO_2	.66	.78	.74	.73	.85	.81	.74	.80	.82	.76	.85
Al_2O_3	16.61	17.85	17.13	17.81	17.67	17.11	17.86	16.91	17.92	17.90	17.75
MgO	2.16	2.19	1.95	2.50	2.79	2.61	2.74	2.58	2.63	4.07	3.41
Fe_2O_3	5.33	5.72	5.18	6.01	6.35	6.07	6.34	5.92	6.07	6.27	6.36
MnO	.08	.08	.08	.08	.10	.09	.10	.08	.09	.10	.10
CaO	4.69	5.76	5.35	5.24	5.96	5.70	5.74	5.60	6.22	5.65	6.27
Na_2O	3.96	4.06	4.38	4.09	4.20	4.25	4.24	4.19	4.09	4.14	4.15
KaO	1.59	1.38	1.34	1.11	1.18	1.29	.99	1.42	1.22	1.06	1.20
PaO_5	.13	.16	.15	.13	.18	.16	.15	.17	.17	.15	.18
Rb	27	27	21	17	19	20	17	20	17	18	13
Sr	427	471	585	513	507	471	532	538	542	544	505
Zr	151	127	133	157	143	137	135	141	133	132	123
Ni	36	17	27	32	41	42	49	42	41	43	43
Sc	11.2	11.3	11.4	11.9	12.9	12.6	12.9	12.9	12.7	13.4	14.1
Co	14.5	14.9	13.3	16.2	18.4	17.6	18.8	17.6	18.0	19.2	19.5
Hf	4.5	3.7	3.8	3.6	3.9	3.7	3.8	4.2	3.7	4.1	3.8
Ta	1.0	.7	.7	.6	.6	.8	.4	n.d.	n.d.	n.d.	.6
U	1.4	1.4	1.1	n.d.	2.6	.9	n.d.	n.d.	1.2	1.0	1.4
Th	4.8	n.d.	3.4	2.4	2.4	2.6	2.3	3.3	2.7	2.5	2.6
Ba	430	309	360	378	249	308	250	358	335	292	298
La	20.4	16.1	18.6	13.7	15.4	15.1	15.0	17.0	16.3	15.8	15.9
Ce	41.8	33.6	36.9	28.4	30.8	32.4	31.9	37.1	34.3	33.4	33.4
Nd	n.d.	n.d.	20	n.d.	n.d.	n.d.	n.d.	n.d.	n.d.	n.d.	n.d.
Sm	4.1	3.9	4.1	3.5	4.0	3.9	3.9	4.0	3.9	3.8	3.9
Ev	1.0	1.1	1.2	1.0	1.2	1.1	1.1	1.1	1.1	1.2	1.1
Tb	n.d.	.6	.5	.4	.6	.7	.5	n.d.	.5	n.d.	.6
Yb	1.2	1.4	.8	.8	1.6	1.0	1.3	1.3	1.2	1.3	1.3
Lu	.3	.2	.2	.2	.3	.2	.2	.2	.2	.2	.2

Table 3--Continued

	Eliot Branch - Cooper Spur Section						Yocum Ridge Section			
	HD-66	HD-67	HD-68	HD-69	HD-74	HD-72	HD-78	HD-79	HD-80	HD-81
SiO_2	62.71	60.58	60.73	60.67	60.90	60.14	59.89	59.27	59.98	63.30
TiO_2	.74	.91	.90	.85	.87	.93	.93	.98	.80	.77
Al_2O_3	17.70	17.22	17.08	17.68	17.28	17.69	18.10	17.65	18.54	17.12
MgO	1.85	2.77	2.74	2.74	2.67	2.66	2.77	3.19	2.78	1.92
Fe_2O_3	5.91	6.20	6.10	6.10	6.18	6.14	6.67	6.70	6.61	5.46
MnO	.09	.09	.09	.10	.10	.09	.10	.10	.11	.09
CaO	5.55	6.06	6.02	5.86	5.92	6.34	6.16	6.45	6.02	5.31
Na_2O	4.16	4.35	4.47	4.25	4.34	4.23	4.29	4.10	4.14	4.27
K_2O	1.14	1.55	1.58	1.47	1.50	1.49	.98	1.33	.86	1.61
P_2O_5	.16	.27	.31	.28	.25	.28	.18	.24	.15	.15
Rb	18	21	25	23	20	19	12	19	13	29
Sr	593	807	811	908	1040	1116	583	679	582	572
Zr	147	185	209	170	160	152	135	150	114	137
Ni	24	23	27	28	27	25	n.d.	n.d.	n.d.	n.d.
Sc	11.6	11.6	11.6	11.6	13.6	11.6	11.9	n.d.	12.5	10.8
Hf	4.0	4.8	4.8	4.7	4.6	4.3	3.5	4.0	3.4	4.3
Ta	1.4	1.8	1.4	1.6	1.4	1.1	1.0	.9	.9	1.3
U	1.4	4.5	1.9	2.1	1.8	1.6	2.9	n.d.	5.2	2.4
Th	3.1	4.8	5.1	4.9	4.4	4.3	1.9	3.1	1.5	3.9
Ba	300	463	436	476	450	496	235	331	200	240
La	17.5	28.3	28.4	28.6	31.5	32.9	13.2	19.3	n.d.	18.6
Ce	36.3	57.7	59.7	58.4	66.4	69.0	36.1	39.3	25.6	39.5
Nd	n.d.	42	n.d.	31	42	44	18	n.d.	n.d.	n.d.
Sm	4.1	5.8	5.8	5.5	6.6	6.5	4.5	4.6	3.5	4.3
Eu	1.2	1.5	1.6	1.5	1.6	1.7	1.2	1.3	1.1	1.0
Tb	.6	.7	.7	n.d.	.6	.5	.5	.6	.5	.5
Yb	1.1	1.3	1.4	1.5	1.3	1.3	1.2	1.2	1.4	1.6
Lu	.2	.2	.2	.2	.3	.2	.2	.2	.2	.3

Table 3--Continued

	Zigzag Canyon - Mississippi Head Section					Mt. Hood Meadows Section					
	HD-89	HD-88	HD-87	HD-86	HD-1	HD-16	HD-15	HD-14	HD-13	HD-12	HD-11
SiO_2	61.43	61.16	60.11	61.85	62.98	59.52	59.96	60.07	59.65	60.55	61.75
TiO_2	.78	.85	.88	.77	.76	.94	.95	.92	.93	.87	.77
Al_2O_3	17.26	17.43	17.78	17.74	16.95	17.87	17.55	17.53	17.59	17.47	17.39
MgO	3.03	2.63	3.06	2.12	2.38	2.80	2.84	2.90	3.07	2.82	2.60
Fe_2O_3	6.34	6.27	6.42	6.36	5.56	7.00	6.79	6.64	6.81	5.92	5.80
MnO	.10	.09	.09	.09	.07	.09	.09	.09	.09	.08	.08
CaO	5.55	5.80	6.23	5.52	5.46	5.99	5.96	5.95	6.12	5.99	5.75
Na_2O	4.15	4.25	3.93	4.16	4.21	4.30	4.22	4.27	4.17	4.51	4.27
K_2O	1.19	1.31	1.34	1.22	1.48	1.26	1.40	1.41	1.36	1.55	1.43
P_2O_5	.16	.21	.16	.17	.16	.23	.25	.22	.23	.24	.17
Rb	23	21	22	21	23	15	20	19	18	18	22
Sr	524	571	580	580	568	596	574	589	562	928	603
Zr	167	154	159	161	158	158	183	175	178	152	150
Ni	n.d.	n.d.	n.d.	n.d.	n.d.						
Sc	12.8	11.6	13.6	11.5	11.5						
Hf	4.3	4.5	4.6	4.0	4.3						
Ta	1.4	1.6	1.4	1.4	.9						
U	1.3	1.3	1.8	1.5	n.d.						
Th	3.2	1.8	3.7	3.3	3.8						
Ba	329	333	310	321	327						
La	20.5	19.2	19.8	18.7	18.1						
Ce	40.1	38.3	39.5	37.7	39.3						
Nd	22	20	20	n.d.	n.d.						
Sm	4.4	4.3	4.4	4.3	4.0						
Eu	1.2	1.2	1.2	1.2	1.1						
Tb	.5	.5	.5	.5	.4						
Yb	1.4	1.5	1.4	1.3	1.0						
Lu	.2	.2	.3	.2	.2						

Table 3--Continued

	Coe Branch - Barrett Spur Section				Langille Crags Section		
	HD-43	HD-46	HD-47	HD-45	HD-75	HD-76	HD-77
SiO_2	63.70	60.19	60.96	62.31	61.95	62.51	60.82
TiO_2	.70	.85	.87	.79	.89	.88	.85
Al_2O_3	17.44	17.77	18.00	17.19	16.98	16.47	17.59
MgO	2.04	2.98	2.61	2.48	2.36	2.35	2.54
Fe_2O_3	4.84	6.44	5.99	5.70	5.70	5.75	6.21
MnO	.07	.09	.07	.08	.08	.09	.09
CaO	5.23	6.05	5.73	5.53	5.81	5.61	5.88
Na_2O	4.33	4.07	4.50	4.23	4.15	4.26	4.30
K_2O	1.50	1.40	1.11	1.53	1.78	1.79	1.46
P_2O_5	.15	.17	.17	.16	.30	.29	.25
Rb	21	24	11	20	23	26	23
Sr	550	575	615	636	927	881	909
Zr	152	177	135	157	197	193	177

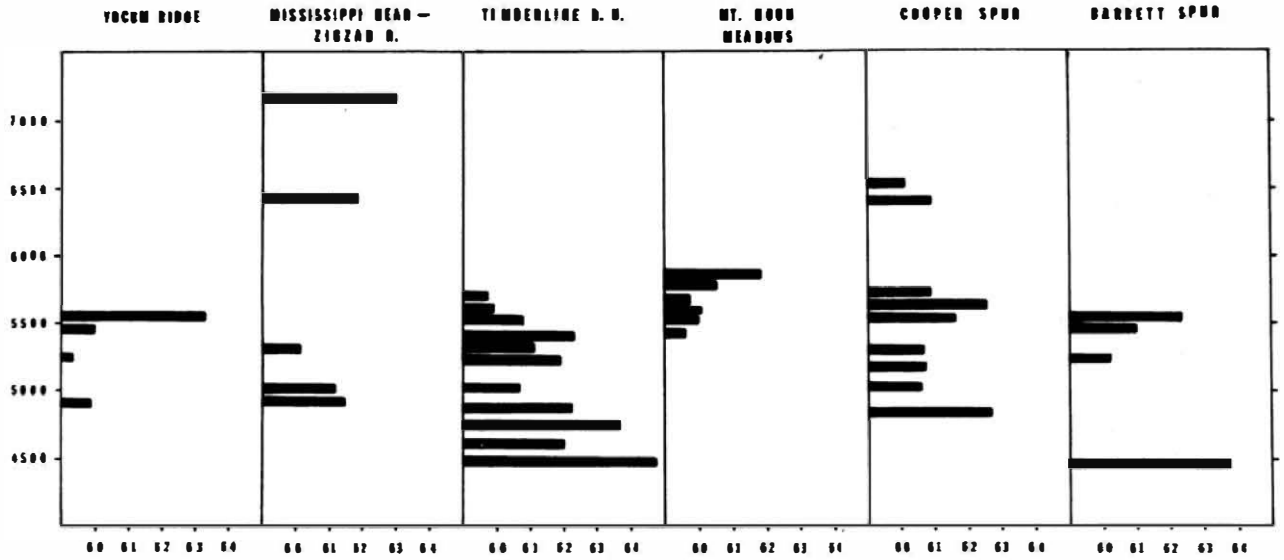

Figure 8: A graph of weight percent silica in Main Stage lavas versus projected stratigraphic height. The surface sections have been projected downdip to a distance from the summit that is equal to that of the Timberline drill hole.

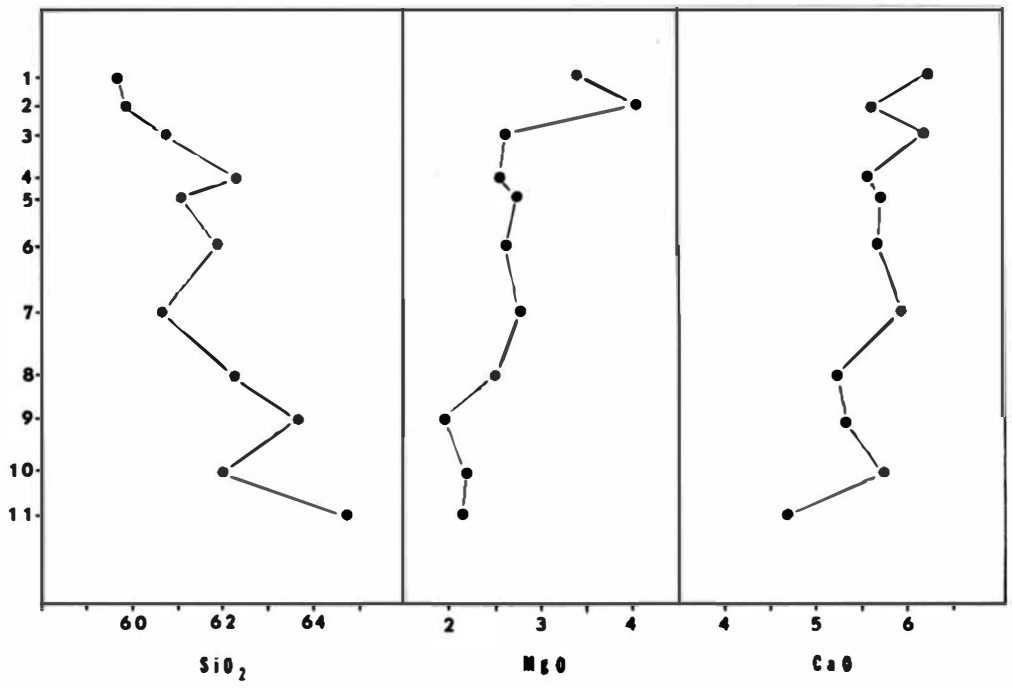

Figure 9: A plot of the concentrations of selected major elements versus flow number for the Timberline drill hole section.

discrete magma batches from several different vents. Those flows that have intermediate concentrations of excluded trace elements may represent separate magma batches or may be mixtures of two or more end-member parent compositions. The variability in abundance of trace elements in lavas with similar SiO_2 contents could be caused by differences in the proportion of partial melting that produced each magma batch. Because of the eutectic nature of partial melting, small differences in the amount of melting would not affect the major element composition of the liquid; however, a parental magma that is produced by a small degree of melting would have considerably higher abundances of the excluded trace elements than one representing a greater proportion of melt.

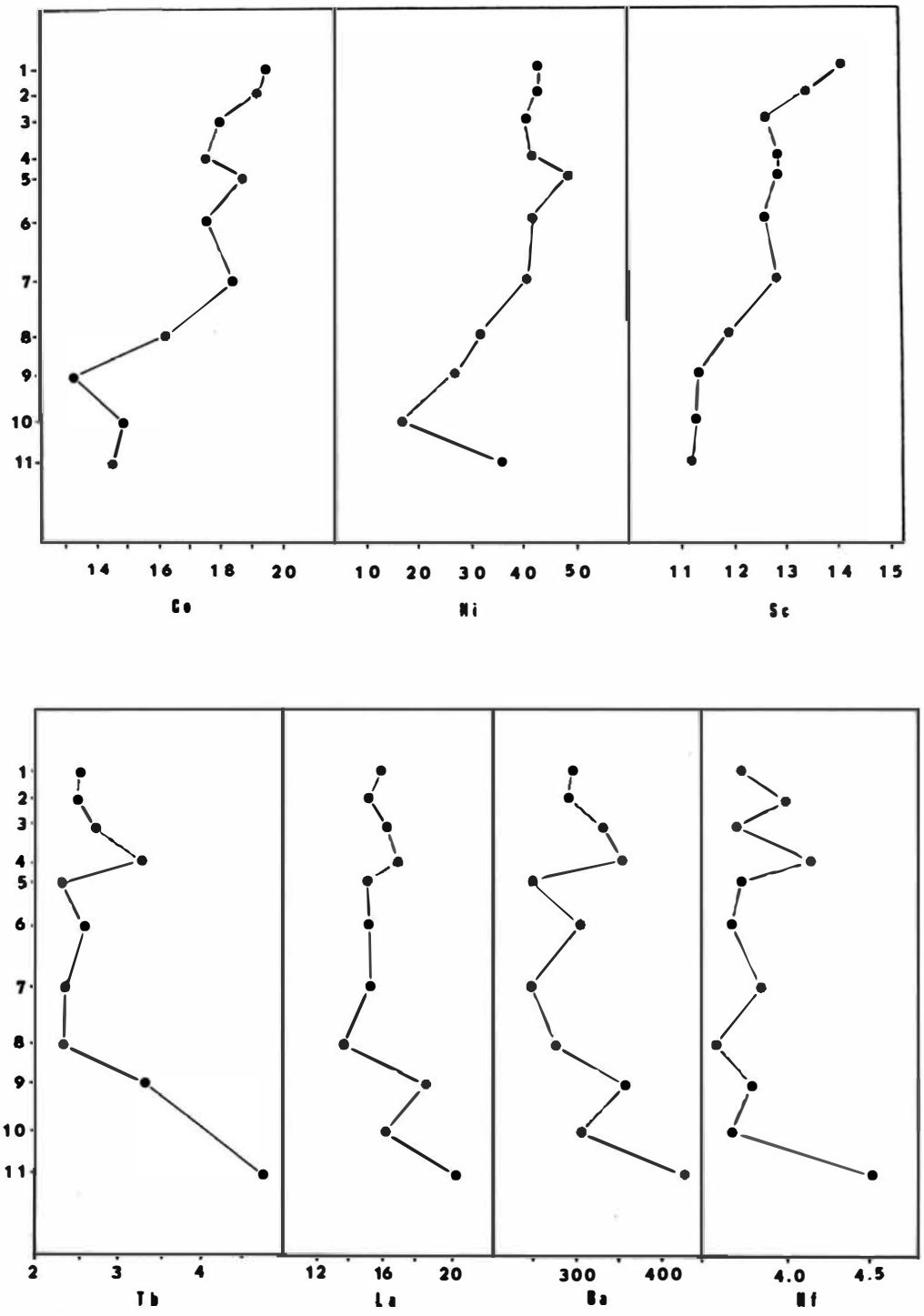

Figure 10: A plot of the concentrations of selected trace elements versus flow number for the Timberline drill hole section.

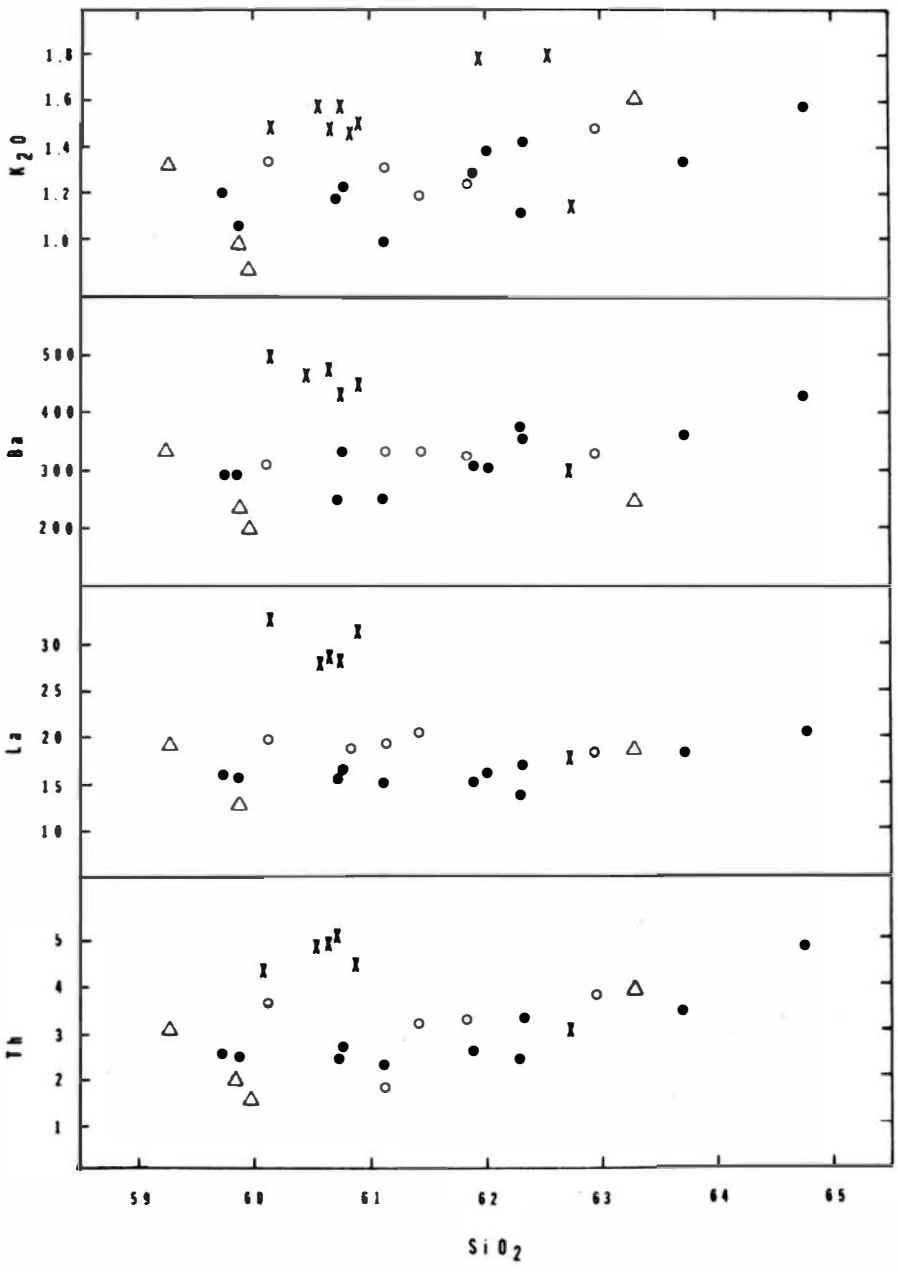

Figure 11: A plot of selected "incompatible" elements versus silica concentration in Main Stage lavas: solid circles = Timberline drill hole section; open circles = Mississippi Head-Illumination Rock section; triangles = Yocum Ridge section; X = Eliot Branch - Cooper Spur section.

SUMMARY AND GEOTHERMAL IMPLICATIONS

The post-glacial silicic lavas were erupted during three temporally distinct episodes, each of which tapped a discrete batch of magma that was being differentiated by small amounts of fractional crystallization. Equilibria calculations indicate that immediately prior to eruption the dacitic magmas were at temperatures of about 935° C and were located at least eight km beneath Mt. Hood.

The Main Stage lavas comprise about 90 percent of the volume of Mt. Hood and, like the young dacites, represent several geochemically distinct magma batches. In contrast to the post-glacial magmas, the Main Stage magmas do not appear to have undergone fractional crystallization during the course of an eruptive episode. Instead, the existence of silica-rich lavas near the base of the Mt. Hood sequence indicates that the Main Stage magma chambers may have been compositionally zoned. It is suggested that processes resulting in zonation of a magma may be more likely to occur in large Main Stage chambers than in those representing the more rapidly cooled, small, post-glacial magma bodies.

The geothermal evaluation of an igneous system is based on the age, volume and depth of possible magma chambers. Smith and Shaw (1975) suggest 10 km as a maximum depth for magma chambers associated with potential geothermal resources. If the late-stage Mt. Hood magmas last equilibrated at depths near 10 km, as suggested by the equilibrium calculations, then residual magma in the chamber may have little influence on near-surface geothermal systems. Because of the young age of the most recent eruptions, a local heat source could be provided by magma that is still residing at shallow depths within the volcanic conduit. Calculations indicate that a cylindrical conduit which has the diameter of the Crater Rock plug dome would contain about 0.3 km^3 of magma in the upper 10 km of its length.

The geothermal significance of the Main Stage volcanism cannot be precisely evaluated because the age and depth of the associated magma chambers is not known. Estimates of the age and volume of the residual magmas indicate that they may still be associated with major geothermal anomalies (Figure 12); however, there is no reason to believe that these magmas are located at shallow depths. Deep-seated magmatic bodies could have considerable effect on the regional geothermal gradient in the Mt. Hood area, although it is unlikely that they would significantly affect the thermal regime of the volcanic edifice. Potential resources associated with a high regional anomaly would more likely be found along deeply penetrating structures.

In summary, the geological and geochemical evidence indicates that geothermal anomalies may exist at two levels in the Mt. Hood area: a shallow, localized anomaly associated with the young volcanic conduit, and a deep, regional anomaly associated with the Mt. Hood magma reservoirs.

ACKNOWLEDGEMENTS

This investigation was carried out under a grant from the Oregon Department of Geology and Mineral Industries and was made possible by the continued interest of Dr. Donald A. Hull, State Geologist. Initiation of the study was greatly facilitated by field trips and discussions with Dwight Crandall and William Wise. I was aided in the field by the climbing expertise and insightful observations of Howard Naslund. Professors Goles, Baker and McBirney of the University of Oregon reviewed the text and offered many helpful suggestions. Carolyn Sherrell provided vital assistance by typing the camera-ready copy.

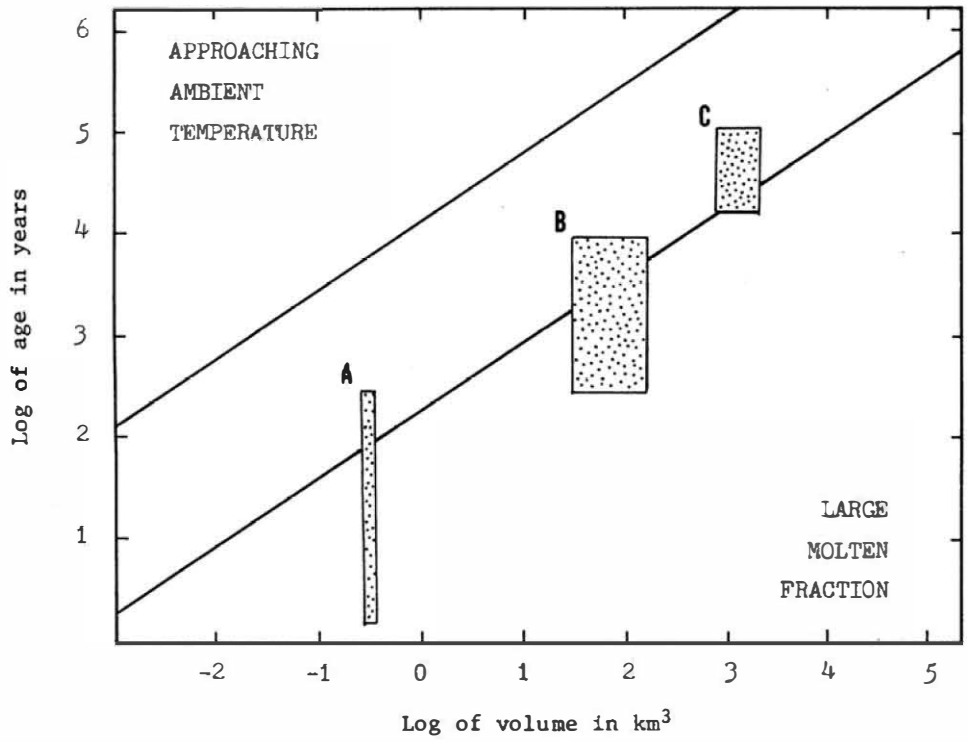

Figure 12: Graph of theoretical cooling time versus volume for magma bodies. Systems having magma chambers with large molten fractions would plot below the diagonal lines; systems that are now approaching ambient temperatures would plot above the diagonal lines; systems that may now be approaching a completely crystallized state would plot between the diagonal lines (after Smith and Shaw, 1975). Field A shows the age and volume range for a shallow volcanic conduit beneath Mt. Hood. Fields B and C show the ranges in age and volume for the post-glacial and Main Stage magma chambers, respectively.

REFERENCES

Buddington, A. F., and Lindsley, D. H., 1964, Iron-Titanium Oxide Minerals and Synthetic Equivalents: J. Petrol, v. 5, p. 310-357.

Crandall, D. R., and Rubin, M., 1977, Late-Glacial and Post-Glacial Eruptions at Mt. Hood, Oregon: Geol. Soc. Am. Abs. with Programs 9, n. 4.

Kudo, A. M., and Weill, D. F., 1970, An Igneous Plagioclase Thermometer: Contrib. Mineral. Petrol., v. 25, p. 52-65.

Smith, R. L., and Shaw, H. R., 1975, Igneous-Related Geothermal Systems, in Assessment of Geothermal Resources of the United States: U. S. Geological Survey Circular 726, p. 58-84.

Thorarinsson, S., 1954, The Tephra Fall from Hekla on March 29, 1947, in The Eruption of Hekla 1947-48, II: Soc. Scient. Islandica., p. 68.

Wise, W. S., 1969, Geology and Petrology of the Mt. Hood area: A Study of High Cascade Volcanism: Geol. Soc. Am. Bull., v. 80, p. 969-1006.

Wood, B. J., and Banno, S., 1973, Garnet-orthopyroxene and orthopyroxene-clinopyroxene Relationships in Simple and Complex Systems: Contrib. Mineral. Petrol., v. 42, p. 109-124.